Numerical Modelling of Soot Formation in Laminar Axisymmetric Ethylene-Air Coflow Flames at Atmospheric and Elevated Pressures

Ahmed Abdelgadir*, Ihsan Allah Rakha*, Scott A. Steinmetz, Antonio Attili, Fabrizio Bisetti, William Roberts

Clean Combustion Research Center, King Abdullah University of Science and Technology, Saudi Arabia

Abstract

A set of coflow diffusion flames are simulated to study the formation, growth, and oxidation of soot in flames of diluted hydrocarbon fuels, with focus on the effects of pressure. Firstly, we assess the ability of a high performance CFD solver, coupled with detailed transport and kinetic models, to reproduce experimental measurements of a series of ethylene-air coflow flames. Detailed finite rate chemistry describing the formation of Polycyclic Aromatic Hydrocarbons is used. Soot is modeled with a moment method and the resulting moment transport equations are solved with a Lagrangian numerical scheme. Numerical and experimental results are compared for various pressures. Finally, a sensitivity study is performed assessing the effect of the boundary conditions and kinetic mechanisms on the flame structure and stabilization properties.

1 Introduction

Carbon particulate formed as a result of combustion or pyrolysis is of great concern. Soot is a combustion inefficiency and an atmospheric pollutant, which poses significant health risks and contributes to long term climate change. Therefore, better understanding of soot formation in combustion processes is required.

Two dimensional axisymmetric laminar diffusion flames are widely used to study soot formation due to their simplicity. Most of the early numerical studies of soot formation in laminar co-flow diffusion flames at atmospheric pressures did not reproduce accurately the distribution of soot volume fraction either along the centerline or along the wings. Smooke et al. [1, 2] predicted the peak soot volume fraction to be along the flame wings whereas in experiments peak soot volume fraction was found along the centerline. They attributed this discrepancy to the simple acetylene based soot model employed and uncertainties in the inlet boundary conditions. Liu et al. [3] reported the same findings for laminar methane-air flames at 1 atm using an acetylene based soot model. Very few numerical studies have been conducted on soot formation in laminar diffusion flames at elevated pressures. Soot formation is predicted to be significantly enhanced with increasing pressure. This increase of soot yield at high pressures is due to the narrowing of the flames, which results in an increase of local temperatures near the centerline and it intensifies the fuel pyrolysis in the central core. Zhang and Ezekoye [4] predicted higher soot concentrations at high pressures as compared to atmospheric conditions, and they linked this increase in soot concentration to an increase in gas phase density. Charest et al. [5] predicted a significant influence of pressure on sooting behavior and flame structure of laminar diffusion flames for up to 5 atm. Their predictions, based on an acetylene based soot model, differed significantly from experimental results. Eaves et al. [6] simulated ethane-air co-flow flames at 2, 5, 10, and 15 atm using a detailed PAH-based sectional soot model. They under-predicted the centerline soot volume fraction by a factor of 2-3 for high pressures. Their results showed an outward radial shift of the peak soot volume fraction location as compared to the experimental data.

In early numerical studies, Smooke et al. [1, 2, 7, 8] did not include the fuel tube in the computational domain. To account for preheating effects, different inlet temperatures of fuel and air streams were used, resulting in variations of up to 100 K in peak flame temperatures for different inlet boundary conditions [1]. Efforts were made to match the inlet boundary conditions, both for fuel and air, at the exit of the nozzle. Guo et al. [9] studied these flames with two different models, with and without the fuel tube, and showed that preheating of the incoming gases due to the radiative flux from the flame and the inclusion of the nozzle have a significant effect on the prediction of soot formation. It has been observed in experiments that heat transfer from the flame to the nozzle might have a significant effect on flame structure, thus affecting the accurate prediction of soot, and other flame characteristics. Gülder et al. [10] experimentally investigated the effect of the fuel tube wall material on the soot formation and the temperature field. Their experiments showed that for different materials, variations of about 200-250 K in flame temperatures occured for propylene flames. This work pointed to the need for proper treatment of the fuel tube in numerical models. Most of the numerical models assume a fixed fuel tube temperature or adiabatic conditions [11, 12]. Comparison of predicted soot volume fraction with experimental results, for two different predictions about fuel tube temperature (fixed

*Corresponding author

Email addresses: ahmed.abdelgadir@kaust.edu.sa (Ahmed Abdelgadir) ihsanallah.rakha@kaust.edu.sa (Ihsan A. Rakha)

Proceedings of The European Combustion Meeting 2015

temperature and adiabatic assumption), have shown that true value lies within these predictions [11, 12]. Modeling of the conjugate heat transfer (CHT) problem involving the fluid streams and the fuel tube is also possible [11], though it comes at a high computational cost.

In the present study, soot simulations for laminar co-flow diffusion ethylene-air flames at 1, 2, and 4 atm are performed to reproduce experimental measurements of a series of ethylene-air co-flow flames [13, 14]. This series is one of the target flame sets of the International Sooting Flame workshop (ISF) [15]. Species and temperature profiles are compared to the experimental measurements for all pressures. Sensitivity of the numerical predictions to fuel tube boundary condition and kinetic mechanisms are assessed.

2 Numerical Methods and Physical Models

Fully coupled unsteady conservation equations for mass, momentum, energy, and species mass fractions are solved using a low-Mach number formulation. Radiative heat transfer is neglected. The in-house code 'NGA', developed at Stanford University, is used. Transport equations are discretized on a structured mesh and solved with a finite difference method. Details on the discretization and numerical methods used to solve momentum and scalar transport equations are given in [16].

2.1 Numerical Configuration and Boundary Conditions

Target flame sets of ethylene-air laminar co-flow diffusion flames of the International Sooting Flame workshop (ISF) are modelled for 1, 2, and 4 atm. Details of experimental setup and techniques to measure temperature, species, and soot volume fraction can be found in [13, 14]. The mass flow rate of the fuel stream is 1.37 mg/s ethylene and 6.41 mg/s nitrogen, and the mass flow rate for the co-flow is 1.25 g/s air. The mass flow rates remain constant at all pressures. The fuel tube has an inner radius of 2 mm and outer radius of 2.5 mm. A constant fuel tube wall temperature boundary condition is implemented. The sensitivity of the numerical results to the fuel tube wall temperature will be discussed later. The domain extends 25 mm in the radial direction, 59 mm above the fuel tube exit and 8 mm below the fuel tube exit plane. The whole domain is divided into 669×169 ($N_x \times N_r$) control volumes distributed non-uniformly in the domain. The uniform smallest mesh size of 100 μm $\times$ 100 μm is used from r=0 mm to r=8 mm in the radial direction and from x=-8 mm to x=12 mm in the axial directions. A time step of 10 μs is used.

2.2 Soot Model

The soot model takes into account nucleation, coagulation, growth (condensation and surface growth), and oxidation. The details of soot model can be found in [16] and references therein. A brief description is presented here. Acetylene, napthalene, acenaphthylene, biphenyl, phenanthrene, acephenanthrene, pyrene, fluoranthene, and cyclopenta[cd]pyrene are taken as the precursors of soot. In the model employed, nucleation occurs as the result of the collision of two PAH dimers and condensation occurs due to collisions between PAH dimers and soot particles. Coagulation is the collision of two soot particles. Growth due to surface reactions is addressed by the H-abstraction/C_2H_2-addition (HACA) mechanism as given in [17]. Two oxidizing species, OH and O_2 are considered. Oxidation by OH is approximated by the collision rate between soot and OH as explained by Neoh et al. [18]. The kinetic rate parameters for oxidation by O_2 are taken from [19]. Soot is modeled with a moment method [20] and the resulting moment transport equations are solved with a Lagrangian numerical scheme [21].

2.3 Chemistry

Two different mechanism have been used: a kinetic mechanism A by Qin et al. [22], that consists of 71 species and 469 reactions and a mechanism B by Narayanswamy et al. [23], with 158 species and 1804 reactions. Employing mechanism A, we computed an unstable flame at 1 atm. The flame blowed off right after ignition. Conversely, for the same conditions, flame was stabilized with the mechanism B. For the two mechanisms, a comparison of laminar premixed flame speeds (S_L) at various inlet stream temperatures is conducted. Figure 1 shows considerable differences of up to 60% in S_L and the difference increases with increasing inlet temperature. The flame speed predicted by the mechanism B is higher than the flame speed predicted by the mechanism A. This difference in flame speeds explains different stabilization behaviors. The lower flame speed predicted by the mechanism A resulted in flame blow off. All the numerical results presented here are based on the detailed kinetic chemical mechanism developed by Narayanswamy et al. [23].

3 Results

3.1 Temperature

Comparisons of predicted temperature and measured temperature profiles are shown in Fig. 2 and Fig. 3. Temperatures are measured with thermocouples and an appropriate radiation correction is applied to the raw data [13]. Comparison of the predicted temperature contours against experimental measurements show that the flame structure is well predicted at all pressures. As the pressure increases, the flame becomes thinner and the peak flame temperature increases. The overall temperature field for each pressure is in reasonable agreement with experimental data. The predicted center-line temperature profiles are in good agreement with the experiments for all pressures. The trends, narrowing of flame and increase in peak flame temperature with increasing pressure are well captured by the simulations. The rise in temperature along the centerline is in reasonable, albeit

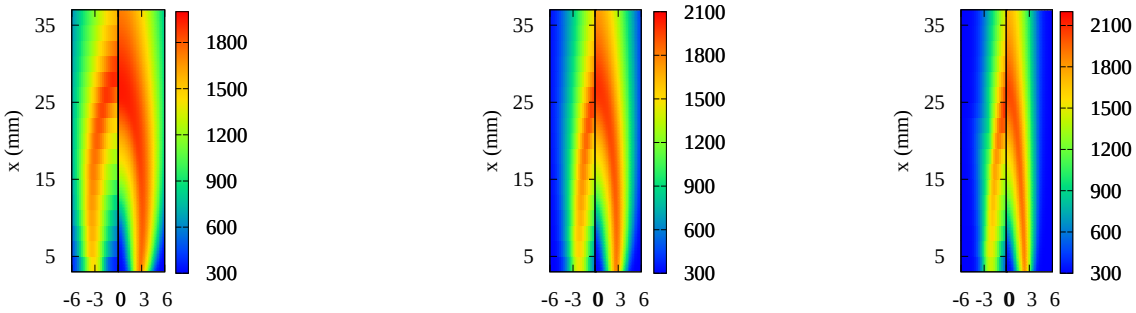

Figure 2: Comparison of measured temperature contours (left side) and predicted temperature contours (right side) for 1 atm (left), 2 atm (middle), and 4 atm (right).

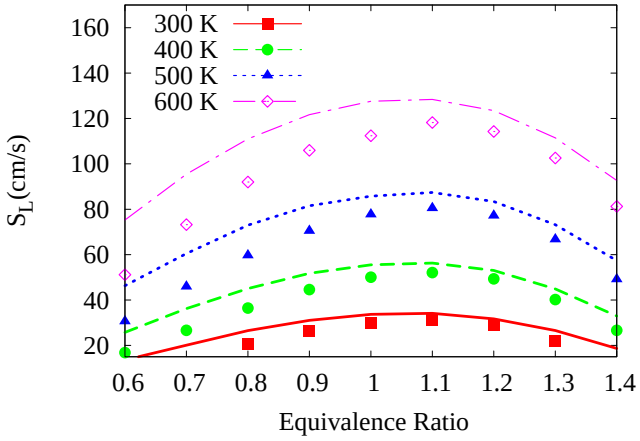

Figure 1: Comparison of flame speed of premixed flames over a range of equivalence ratios at different inlet temperatures for two different mechanisms:Narayanaswamy et al. [23] (lines) and Qin et al. [22] (symbols).

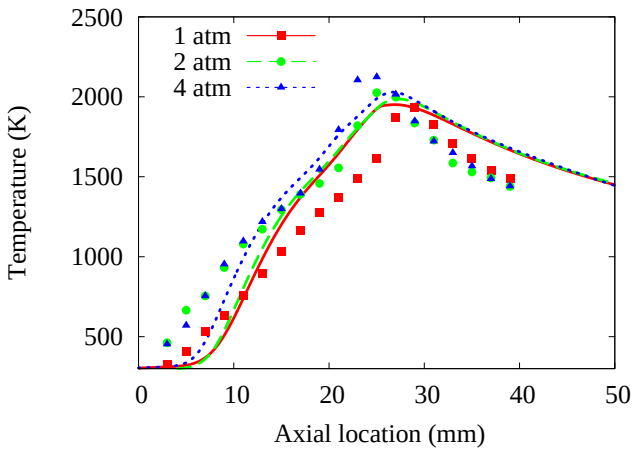

Figure 3: Predicted (lines) and measured (symbols) centerline temperature profiles at 1 (red-square), 2 (green-circle), and 4 atm (blue-triangle).

not perfect agreement relative to experimental measurements along centerline. Differences between measured and computed temperatures exist for up to 300 to 400 K. Flame height taken as the location of peak temperature along the centerline is found to be about 2.7 cm for all pressures which is in good agreement with the experimental measured flame height. The variation in flame height as pressure is increased from 1 to 4 atm is negligible, which is consistent with the experimental findings.

3.2 Sensitivity of the Fuel Tube Wall Boundary Conditions

A constant temperature (T_w) boundary condition is prescribed for the fuel tube wall. To analyze the sensitivity of the flame structure to the tube wall temperature, three simulations with different boundary wall temperatures are performed. Flame stabilization and flame structure are found to be sensitive to the tube temperature as

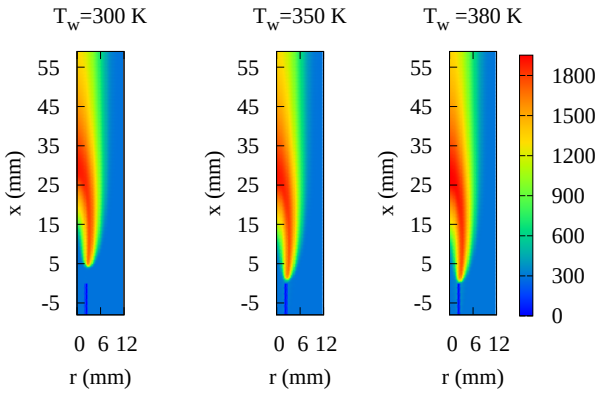

Figure 4: Temperature contours with three different fuel tube wall temperature boundary conditions (T_w=300, 350, and 380 K) at 1 atm.

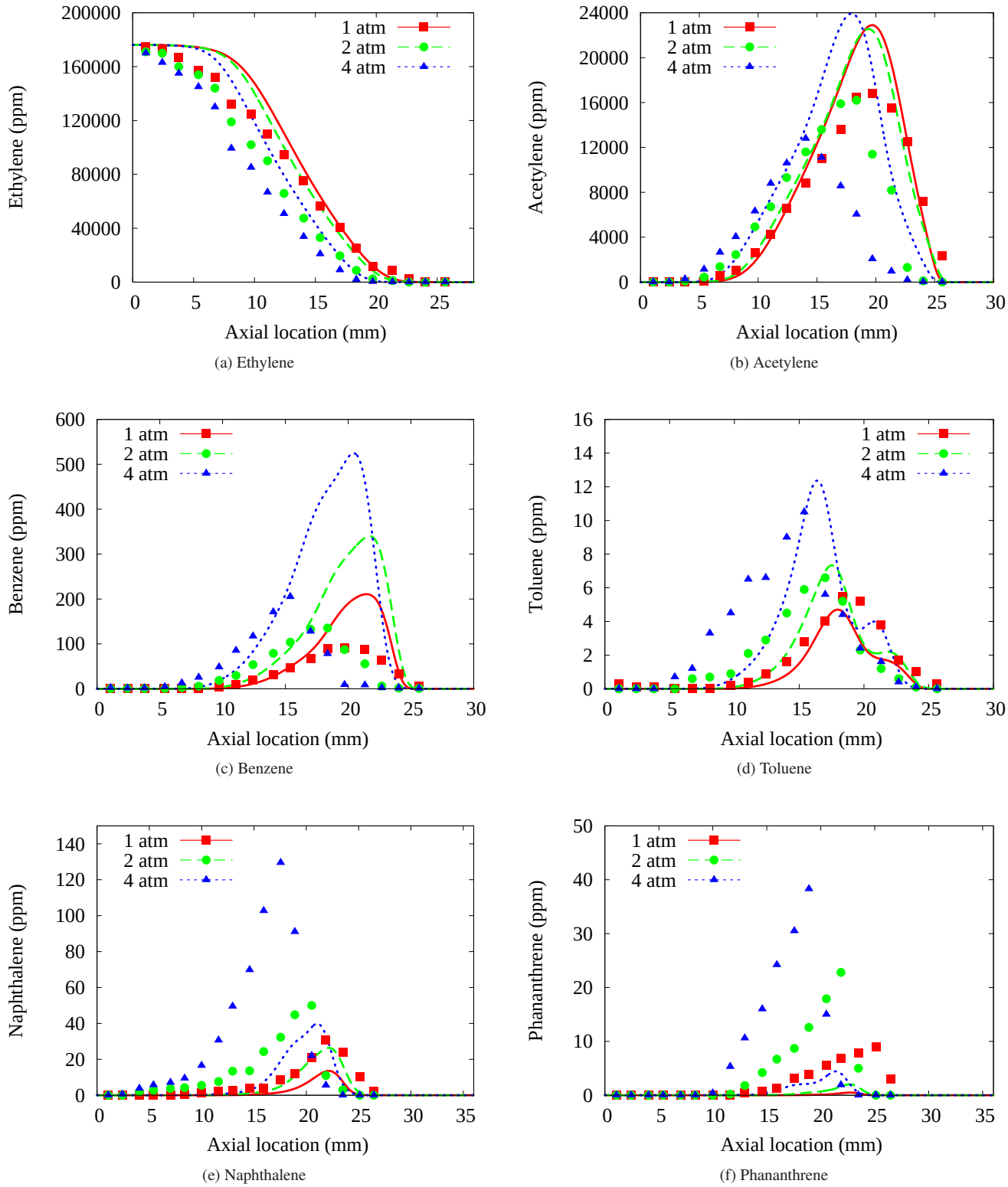

(a) Ethylene (b) Acetylene

(c) Benzene (d) Toluene

(e) Naphthalene (f) Phananthrene

Figure 5: Measured (symbols) and predicted (lines) centerline profiles for species mass fractions at 1 (red-square), 2 (green-circle), and 4 atm (blue-triangle).

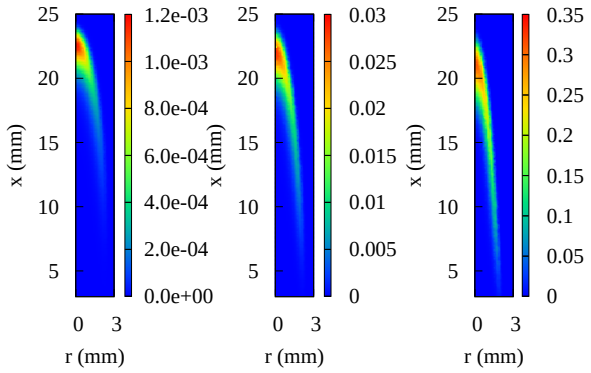

Figure 6: Soot volume fraction f_v (ppm) for 1 atm (left), 2 atm (middle), and 4 atm (right).

shown in Fig. 4. The computed flame is lifted, with lift-off height of about 4 mm, for $T_w = 300$ K and attached for $T_w = 350$ K, and 380 K. In the remainder of the paper, all results consider a wall temperature for which an attached flame is obtained, in agreement with experimental results. Once the flame is attached, changing the fuel tube wall temperature did not affect the temperature and species profiles.

3.3 Species Mass Fractions

A comparison of the prediced centerline species mass fractions with experimental measurements is presented in Fig. 5. In general, the trends are well reproduced by the calculations with the exception of the acetylene profile. The peaks of all species profiles are shifted upstream with increasing pressure, in agreement with experimentals. Consumption rate of ethylene along centerline increases with increasing pressure as evident from experimental centerline profiles. Naphthalene and phanathrene are under predicted by a factor of about 3-5 and 8-12, respectively. For ethylene, acetylene, benzene, and toluene, the centerline values are over-predicted. Significant over-prediction of acetylene and benzene by a factor of about 2-3 may be related to the under-prediction of naphthalene and phananthrene, as acetylene and benzene are the precursors of polycyclic aromatic hydrocarbons (PAHs). Formation of naphthalene and phananthrene along centerline is delayed relative to experimental data. Predicted peaks of both PAHs along centerline are shifted by about 8 mm relative to experimental profiles.

3.4 Effect of Pressure on Soot Formation

Contours of soot volume fraction (f_v) in ppm are shown in Fig. 6. Soot volume fraction shows a significant sensitivity to the pressure. The location of the peak soot volume fraction is on the centerline for all pressures. If the pressure is increased from 1 to 2 atm, the peak soot volume fraction along the centerline of the flame increases by a factor of 20. If the pressure is increased from 2 to 4 atm, the peak soot volume fraction increases by a factor of 10, showing a transition from lightly to heavily sooting flame. The same behavior is evident from the experimental visualization. Peak soot volume fraction is under-predicted by a factor of 10 as compared to measured peak soot volume fraction at 4 atm. This significant difference can be attributed to the under-prediction of soot precursors. The narrowing of the flame with the increase in pressure can also be observed. As pressure increases, soot formation along the wings becomes more prominent, even though most of the soot is formed at the flame tip. These findings are in qualitative agreement with experimental observations.

4 Conclusions

A series of laminar co-flow diffusion ethylene-air diffusion flames are simulated and compared with the experimental measurements at 1, 2, and 4 atm. This series is one of the target flame sets of the International Sooting Flame workshop (ISF) [13–15].

A reasonable agreement is observed for flame height, temperature, and various species' concentrations. Numerical results show a strong sensitivity of soot volume fraction to pressure. If the pressure is increased from 1 to 2 atm, the peak soot volume fraction near the tip of the flame increases by a factor of 20. If the pressure is increased from 2 to 4 atm , the peak soot volume fraction increases by a factor of about 10, showing a transition from lightly to heavily sooting flame. The same behavior is also evident analyzing experimental visualizations that reveal transition from a slightly luminous to a very bright flame. In all cases, peak soot volume fraction is located along the centerline as observed in the experiments. A detailed analysis shows that the fuel tube wall temperature has an effect on flame stabilization. Moreover, significant differences in the flame stability and propensity to blow-off are found, using two well validated chemical kinetic mechanisms.

References

[1] C. McEnally, A. Schaffer, M. Long, L. Pfefferle, M. Smooke, M. Colket, R. Hall, Twenty-Seventh Symp. (Inter.) Combust. Ins. 27 (1998) 1497–1505.

[2] M. Smooke, C. McEnally, L. Pfefferle, R. Hall, M. Colket, Combust. Flame 117 (1999) 117–139.

[3] F. Liu, H. Guo, G. Smallwood, Combust. Flame 138 (2004) 136–154.

[4] Z. Zhang, O. Ezekoye, CST 137 (1998) 323–346.

[5] M. Charest, C. Groth, O. Gülder, Combust. Flame 158 (2011) 1933–1945.

[6] N. Eaves, A. Veshkini, C. Riese, S. Dworkin, M. Thomson, Combust. Flame 159 (2012) 3179–3190.

[7] M. Smooke, P. Lin, J. Lam, M.B.Long, Twenty-Third Symp. (Inter.) Combust. Ins. 23 (1991) 575–582.

[8] M. Smooke, V. Giovangigli, Imp. Comput. Sci. Engg. 4 (1992) 46–79.

[9] Hongsheng, F. Liu, G. Smallwood, O. G$\ddot{u}$lder, Combust. Theor. Model. 6 (2002) 173–187.

[10] O. G$\ddot{u}$lder, K. Thomson, D. Snelling, Combust. Flame 144 (2006) 426–433.

[11] N. Eaves, M. Thomson, S. Dworkin, Combust. Sci. Technol. 185 (2013) 1799–1819.

[12] M. Charest, O. G$\ddot{u}$lder, C. Groth, Combust. Flame 161 (2014) 2678–2691.

[13] R. K. Abhinavam Kailasanathan, T. L. Yelverton, T. Fang, W. L. Roberts, Combustion and Flame 160 (2013) 656–670.

[14] R. K. Abhinavam Kailasanathan, E. K. Book, T. Fang, W. L. Roberts, Proceedings of the Combustion Institute 34 (2013) 1035–1043.

[15] International sooting flame workshop, `http://www.adelaide.edu.au/cet/isfworkshop/data-sets/pressurised/`, 2012. Accessed: 2015-01-13.

[16] F. Bisetti, G. Blanquart, M. E. Mueller, H. Pitsch, Combustion and Flame 159 (2012) 317–335.

[17] M. Frenklach, H. Wang, Proc. Combust. Inst. 23 (1990) 1559–1566.

[18] K. Neoh, J. Howard, A. Sarofim, in: Particulate Carbon, Springer, 1981, pp. 261–282.

[19] A. Kazakov, H. Wang, M. Frenklach, Combust. Flame 100 (1995) 111–120.

[20] M. Mueller, G. Blanquart, H. Pitsch, Combustion and Flame 156 (2009) 1143–1155.

[21] A. Attili, F. Bisetti, Computers & Fluids 84 (2013) 164–175.

[22] Z. Qin, V. V. Lissianski, H. Yang, W. C. Gardiner, S. G. Davis, H. Wang, Proceedings of the Combustion Institute 28 (2000) 1663–1669.

[23] K. Narayanaswamy, G. Blanquart, H. Pitsch, Combustion and Flame 157 (2010) 1879–1898.